Three-dimensional electron diffraction of plant light-harvesting complex

Da Neng Wang and Werner Kühlbrandt
European Molecular Biology Laboratory, Meyerhofstraße 1, D-6900 Heidelberg, Germany

ABSTRACT Electron diffraction patterns of two-dimensional crystals of light-harvesting chlorophyll *a*/*b*-protein complex (LHC-II) from photosynthetic membranes of pea chloroplasts, tilted at different angles up to 60°, were collected to 3.2 Å resolution at −125°C. The reflection intensities were merged into a three-dimensional data set. The Friedel *R*-factor and the merging *R*-factor were 21.8 and 27.6%, respectively. Specimen flatness and crystal size were critical for recording electron diffraction patterns from crystals at high tilts. The principal sources of experimental error were attributed to limitations of the number of unit cells contributing to an electron diffraction pattern, and to the critical electron dose. The distribution of strong diffraction spots indicated that the three-dimensional structure of LHC-II is less regular than that of other known membrane proteins and is not dominated by a particular feature of secondary structure.

INTRODUCTION

The light-harvesting chlorophyll *a*/*b*-protein complex (LPC-II) associated with photosystem II is an integral membrane protein from chloroplast thylakoids of higher plants. It functions as the major antenna of solar energy and is involved in the regulation of photosynthesis and in the interaction between membranes (for reviews, see Staehelin, 1986; Thornber, 1986; Kühlbrandt, 1987). Each LHC-II polypeptide of 25,000 Da binds 15 molecules of chlorophyll *a* and *b* (Butler and Kühlbrandt, 1988). The isolated complex is stable as a trimer in detergent solution.

We have grown large, well-ordered, two-dimensional (2D) crystals of LHC-II, measuring up to 10 μm in diameter (Kühlbrandt et al., 1983; Wang and Kühlbrandt, 1991). Electron microscopy and image analysis of negatively-stained 2D crystals at 16 Å (1 Å = 0.1 nm) resolution indicated that the complex crystallized as a trimer and showed that the crystals had *p*321 layer group symmetry, with a thickness of ~60 Å (Kühlbrandt, 1984). The unit cell contained two LHC-II trimers, related by a crystallographic two-fold axis in the membrane plane.

2D crystals prepared for electron microscopy in the presence of tannin diffracted to high resolution and were thus suitable for structure determination by electron diffraction, cryo-electron microscopy and image processing. The structure of the complex in projection was determined at 3.7 Å resolution (Kühlbrandt and Downing, 1989) and, more recently, at 3.4 Å resolution (Wang and Kühlbrandt, 1991). Tannin, glucose and vitrified buffer were all able to preserve high-resolution detail of LHC-II. However, tannin proved to be 10–20 times more effective than the other two media (Wang and Kühlbrandt, 1991) and was therefore chosen for 3D data collection.

Baldwin and Henderson (1984) pointed out the importance of the flatness of the support film for electron diffraction at high tilt angles. They found that long-range curvature of the films and, hence, of the 2D crystals causes blurring of high-resolution diffraction spots far from the tilt axis which made it difficult to measure their intensities accurately. With 2D crystals of LHC-II which diffract less strongly than other, comparable specimens, we observed that in addition, the short-range surface roughness of the support film was critical. A surface roughness (defined as the average distance of peaks and valleys from a best-fit surface) of ~2 Å was sufficient to cause blurring similar to that caused by the long-range curvature of the support film (Butt et al., 1991). A simple method of producing atomically flat carbon films was devised and enabled us to record high resolution diffraction patterns of 2D crystals at high tilt angles. In the present paper, we describe the three-dimensional electron diffraction of LHC-II to 3.2 Å resolution. This provided the structure factor amplitudes for determining the 3D structure of LHC-II at 6 Å resolution by electron crystallography which is reported elsewhere (Kühlbrandt and Wang, 1991).

MATERIALS AND METHODS

2D crystallization

LHC-II was isolated (Kühlbrandt et al., 1983) and 2D crystals were grown as described (Wang and Kühlbrandt, 1991). Briefly, the complex

was precipitated from concentrated stock solution in Triton X-100. The precipitate was resolubilized with 0.11% (w/v) Triton X-100 and 0.24% (w/v) *n*-nonyl-ß-D-glucopyranoside at a final chlorophyll concentration of 0.78 mg/ml. 2D crystals of LHC-II formed during a two-stage incubation, first at 25°C for 48 h and then at 35–40°C for 2 h.

Specimen preparation and electron diffraction

Thin carbon films with a thickness of ~100 Å and minimal surface roughness were made by multiple evaporation of carbon rod onto mica in an Edwards 306 evaporator (Edwards High Vacuum, West Sussex, England) (Butt et al., 1991). Specimens were prepared for electron microscopy and electron diffraction in the presence of 0.5% (w/v) tannin of pH 6.0, using the lens technique as described previously (Wang and Kühlbrandt, 1991). The grid was then placed in a Gatan cold-transfer stage (Gatan Inc., Pleasanton, CA) with a tilt range of ±60°. Electron diffraction patterns were recorded at a specimen temperature of −125°C in a JEOL 2000EX electron microscope (JEOL Ltd., Akishima, Tokyo, Japan) operated at 100 kV. A Gatan Television Image Intensifier set at maximum sensitivity and contrast was used to search for crystals in the defocused diffraction mode, with the filament current turned down to minimize radiation damage. The dose rate under such conditions was $\sim 7 \times 10^{-4}$ electrons/Å^2/s. The filament current was turned up after the camera shutter had opened. Exposure times ranged from 16 to 32 s. The nominal camera length was 120 cm. One diffraction pattern was recorded of each crystal onto Kodak SO-163 film by the method of Unwin and Henderson (1975). Films were developed in full strength Kodak D19 developer (Eastman Kodak Company, Rochester, NY) for 12 min. The electron dose to which a crystal was exposed before and during the recording of a diffraction pattern was determined from Kodak SO-163 films exposed with the same dose in imaging mode using the characteristic curves (optical density vs log [dose]) supplied by the company (Kodak Data Release P-252, 1981). The majority of diffraction patterns was collected at 60°. Others were recorded at tilt angles of 0°, 20°, and 45°.

At 200 kV, the absolute values of cross-sections for inelastic and elastic electron scattering become smaller. As a result, it was difficult to detect crystals. Since there was no apparent improvement of the electron diffraction patterns, all data were recorded at 100 kV. However, higher acceleration voltages should be preferable for collecting data at a resolution better than 3 Å because the Ewald sphere is flatter.

Processing of diffraction patterns and data merging

Selected diffraction patterns with uniformly sharp reflections at high resolution were digitized on a microdensitometer (model 1010-GM, Perkin-Elmer Corporation, Gardon Grove, CA) in 2,048 steps by 2,048 steps at 15 μm step size with a square, 15 × 15-μm aperture. The lattice was indexed on the screen of a DEC workstation (model 3200, Digital Equipment Corporation, Maynard, MA) with a program written by K. Leonard (EMBL, Heidelberg). Data processing and other calculations were performed with a VAX computer cluster including a VAX 6000-420. Diffraction data were processed and merged using programs written by Henderson and coworkers (Baldwin and Henderson, 1984; Ceska and Henderson, 1990). The lattice was corrected for spatial distortions such as pincushion and spiral distortion and for the curvature of the Ewald sphere. Background subtraction was carried out for the scattering from the carbon support film and for local variations of background intensity.

To evaluate the quality of reflection intensities from each film, a Friedel *R*-factor, R_{sym}, was calculated (Baldwin and Henderson, 1984):

$$R_{sym} = \frac{\sum_{h,k,z^*} |I_{h,k,z^*} - I_{-h,-k,-z^*}|}{\sum_{h,k,z^*} (I_{h,k,z^*} + I_{-h,-k,-z^*})}, \quad (1)$$

where I_{h,k,z^*} and $I_{-h,-k,-z^*}$ were the intensities of a pair of reflections related by Friedel symmetry. The *R*-factor was a measure of the average ratio between the intensity difference and the mean of reflections related by Friedel symmetry.

Reflection intensities were merged, starting from low tilt angles and gradually including patterns at higher tilt angles, by minimizing the merging *R*-factor R_m of each pattern, calculated according to Baldwin and Henderson (1984):

$$R_m = \frac{\sum_{h,k,z^*} |I_{h,k,z^*obs} - I_{h,k,z^*merged}|}{\sum_{h,k,z^*} I_{h,k,z^*merged}}, \quad (2)$$

where $I_{h,k,z^*merged}$ was the averaged intensity at every lattice point after merging. The *R*-factor served to characterize the average difference between the intensities from each film compared to the merged data set, and provided a measure of the consistency between data from different films. The following parameters were refined in every merging cycle: temperature factor, scaling factor, and, for tilt angles up to 45°, tilt angle and position of tilt axis (Ceska and Henderson, 1990). The refinement of tilt angle and tilt axis of crystals tilted by more than 45° did not improve R_m, and therefore was omitted. The position of the tilt axis and the tilt angle were determined initially by the algorithm of Shaw and Hills (1981). Reflections of each new film were divided into six resolution zones for calculating the overall scaling factor and the temperature factor. The temperature factor was calculated in two different ways (isotropic for tilt angles up to 45°; anisotropic for higher tilts) according to Ceska and Henderson (1990). A two-dimensional data set at 3.2 Å resolution, obtained by merging 0° tilt patterns, provided the starting point for merging diffraction patterns of tilted 2D crystals (Wang and Kühlbrandt, 1991). After each cycle of merging, smooth curves were fitted to the merged data set with a sampling of 1/350 Å^{-1}, which then served as a reference for the next cycle. A set of intensities with indices of (h, k, l) was obtained by sampling the final set of lattice lines at 1/140 Å^{-1}, which was more than adequate to follow the variations of structure factor amplitudes of an object measuring 60 Å in thickness.

Error analysis of intensity measurements

The validity of the kinematic approximation for electron diffraction at 100 kV acceleration voltage of an unstained protein crystal with a thickness of < 100 Å has both been deduced from theory and shown experimentally (Ho et al., 1988; Glaeser and Ceska, 1989). Thus, for a perfect crystal, the average intensity of reflections $\langle I \rangle$ is proportional to the number of the unit cells in the irradiated crystal volume, N_x, and to the number of atoms per volume, n_a (Blundell and Johnson, 1976):

$$\langle I \rangle \propto \frac{V_x}{V_0} \times I_0 \times t \times n_a \times f^2$$
$$\propto I_0 \times t \times N_x \times n_a \times f^2, \quad (3)$$

where I_0 is the incident intensity, t the exposure time, V_x the irradiated

volume of the crystal, V_0 the volume of the unit cell, and f the average atomic scattering amplitude. $I_0 \times t$ is the total electron dose. The standard deviation of the reflection intensity is proportional to the square root of the average intensity, $\sigma(I) \propto \sqrt{\langle I \rangle}$, if the measurements are assumed to obey the Gaussian distribution.

When, as in this case, the number of measurements is large, the average difference between the observed and the merged intensities is $0.798 \times \sigma(I)$ (Korn and Korn, 1968). Therefore, from Eqs. 1 or 2, and from the relation $\sigma(I) \propto \sqrt{\langle I \rangle}$, we have,

$$R = \frac{0.798 \times \sigma(I) \times N_r}{\langle I \rangle \times N_r} \propto \frac{1}{\sqrt{\langle I \rangle}} \propto \frac{1}{\sqrt{n_e}}, \quad (4)$$

where N_r is the total number of reflections and n_e the number of electrons contained in an average reflection. For a two-dimensional crystal of one unit cell thickness, N_r is proportional to the irradiated area of the crystal, A. Substituting 3 into 4,

$$R \propto \frac{1}{\sqrt{(I_0 \times t \times n_a \times f^2 \times A/A_0)}} \propto \frac{\sqrt{A_0}}{f \times D \times \sqrt{(I_0 \times t \times n_a)}}, \quad (5)$$

where A_0 is the area of the unit cell in projection and D the diameter of the irradiated area. It follows that the accuracy of the diffraction measurement is inversely proportional to the diameter of the irradiated area, the average atomic scattering factor, and to the square root of the electron dose and of the number of the atoms per unit cell. Note that Eqs. 4 and 5 are valid for both R_{sym} and R_m of a single pattern. Merging diffraction patterns and averaging intensities of symmetry-related reflections will, in effect, increase the total number of contributing unit cells. Therefore, for a set of merged intensities, R_m decreases as more patterns are merged, and with the degree of crystallographic symmetry.

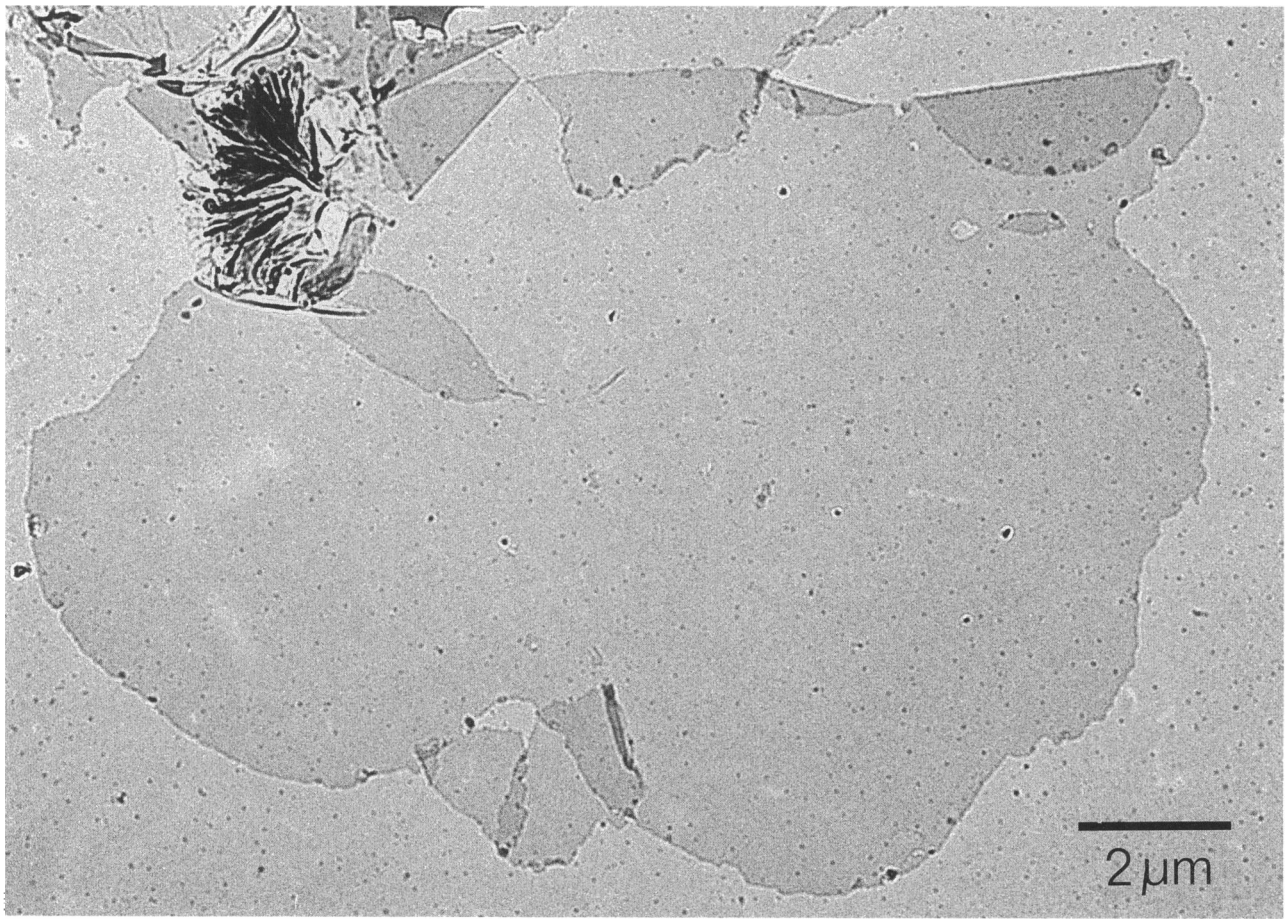

FIGURE 1. Electron micrograph of a two-dimensional crystal of LHC-II measuring about 8 µm × 12 µm. Crystals were grown from the complex solubilized in Triton X-100 and *n*-nonyl-ß-D-glucopyranoside and prepared for electron microscopy and electron diffraction in the presence of 0.5% tannin. The support carbon film had a thickness of ~100 Å.

RESULTS AND DISCUSSION

Diffraction patterns

2D crystals of LHC-II used for electron diffraction measured 6–10 μm in diameter (Fig. 1). Diffraction spots of 2D crystals of LHC-II were generally not visible on the screen of the electron microscope, or even with the assistance of an image intensifier, but could be recorded on film at low specimen temperature. When the Gatan cold stage was kept at a temperature $< -140°$, a thin layer of ice occasionally formed on the grid. The (111) and the (220) diffraction rings of cubic ice were used to determine the precise lattice dimensions of the 2D LHC-II crystals. Taking $d_{111} = 3.66$ Å and $d_{220} = 2.24$ Å (Dubochet et al., 1988), the lattice dimensions of 2D LHC-11 crystals were found to be $a = b = 129.8 \pm 0.2$ Å. This value is slightly larger than those determined previously at room temperature by electron diffraction using purple membrane as an external standard (127 Å; Kühlbrandt, 1987) and by low-angle x-ray scattering of oriented pellets of 2D crystals (128.3 Å; Kühlbrandt, 1988). Because ice formation is undesirable for electron diffraction, the specimen was normally kept at $-125°$

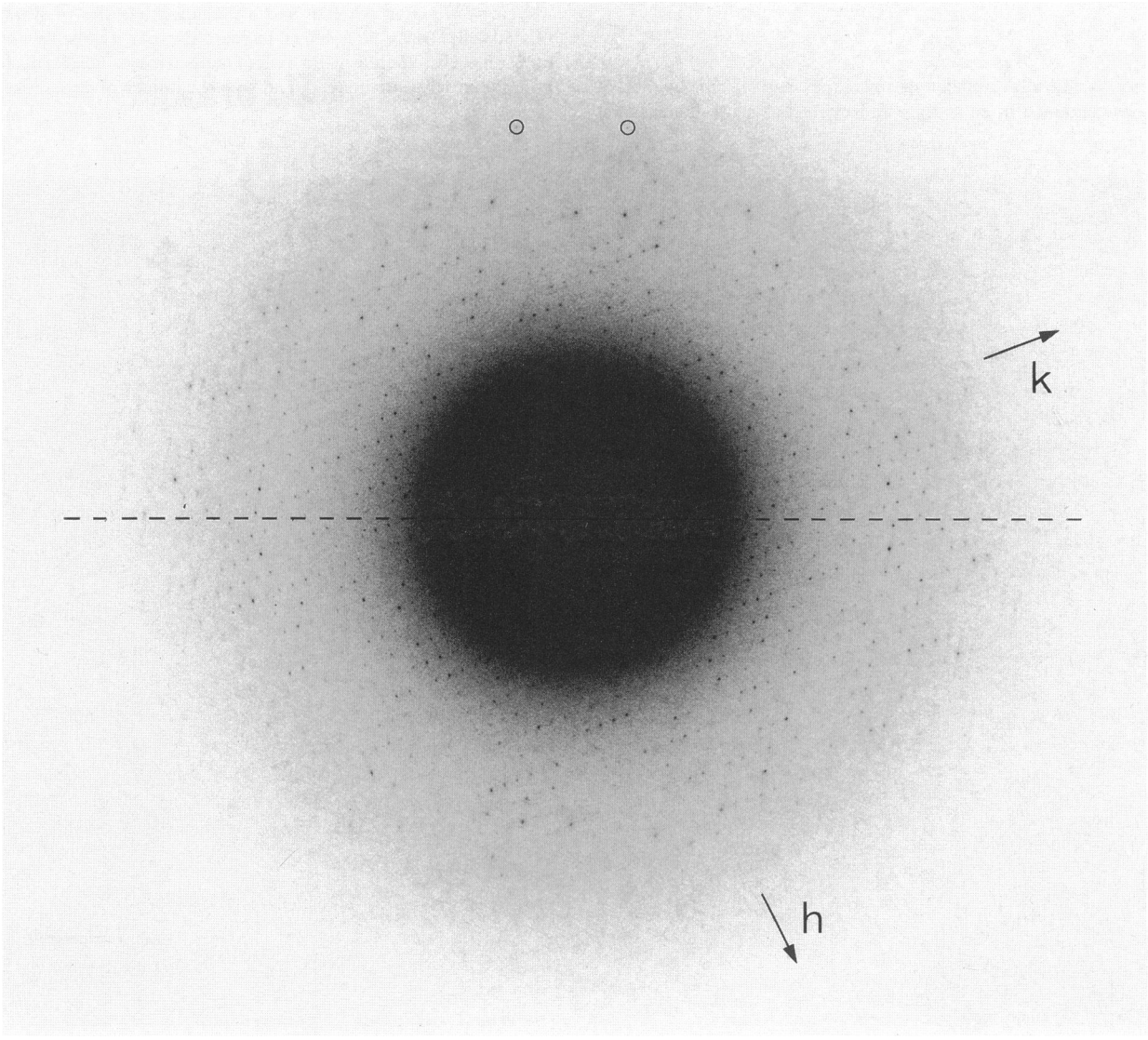

FIGURE 2. Electron diffraction pattern recorded from a two-dimensional crystal of LHC-II tilted by 60° at a temperature of −125°C. The electron dose was ~5 electrons/Å^2. The pattern contains ~1,050 pairs of reflections. The dashed line represents the direction of the tilt axis. Diffraction spots are visible to 3.3 Å resolution along the tilt axis, and to 3.7 Å in the perpendicular direction (*circled*). The spots are almost uniformly sharp, indicating that the curvature of support film was <0.5° and the surface roughness <2 Å. The film was prepared by multiple evaporation of carbon.

and all diffraction patterns were recorded at this temperature.

Fig. 2 is an electron diffraction pattern recorded from a 2D crystal tilted by 60°. It contains ~1,050 pairs of reflections, roughly half as many as an untilted pattern, because the area of the unit cell in projection is smaller by a factor of 2. Spots are almost perfectly sharp in all directions. In our best session, 30% of the patterns at 60° tilt were of this quality. The success rate for isotropically sharp diffraction patterns increased with decreasing tilt angle. At 0° tilt, it was 90% (Wang and Kühlbrandt, 1991).

Diffraction patterns such as the one shown in Fig. 2 can only be recorded with 2D crystals that are nearly perfectly flat. Such specimens are not easy to prepare because large 2D crystals are highly susceptible to distortion. Deviations from planarity are particularly noticeable at high tilt angles where they cause spots far from the tilt axis to spread around the ideal lattice positions. In addition to the requirements for recording high-resolution diffraction patterns of untilted crystals (Wang and Kühlbrandt, 1991), three other factors therefore needed careful control.

First, it was necessary for both surfaces of the carbon support film to be atomically flat. Only the smoothest films, prepared by multiple evaporation (Butt et al., 1991) yielded diffraction patterns of 2D crystals of LHC-II with uniformly sharp reflections at high resolution. Second, the long-range curvature of the carbon film needed to be less than 0.5° over the diffracted area (Butt et al., 1991) which measured 8 μm or more in diameter (see below). We obtained an acceptable yield of 2D crystals of minimal curvature by preparing each grid freshly with a small piece of carbon film floated off its mica substrate (Wang and Kühlbrandt, 1991). Crystals were deposited on the side of the carbon film that had been in contact with the mica. In practice, no specimen was perfectly planar so that high-resolution, off-axis spots were always blurred to some small extent. Third, only the largest 2D crystals were selected for electron diffraction at high tilt angles, to maximize the signal-to-noise ratio. Crystals >8 μm gave diffraction patterns of acceptable quality.

Processing and merging of diffraction data

At 100 kV and 120 cm camera length, the diffraction pattern of a LHC-II crystal covered an area of ~3 cm across on the film. Every diffraction spot measured ~120 μm in diameter, with a closest distance of ~500 μm from one another. Scanning the film with a step size of 15 μm yielded a sampling of 8 × 8 for every reflection. A larger step size (e.g., 20 μm) was found to result in less accurate measurements and an increased R_{sym}. Good separation between adjacent spots was necessary to ensure accurate background measurement. Altogether, 83 out of about 1,200 diffraction patterns of tilted 2D crystals were selected for processing, including 18 of untilted crystals, seven at 20° tilt, ten at 45° and 48 at 60° (Table 1).

In all, there were 93,180 pairs of measured reflections. Of these, 33% had an intensity of more than twice the average difference between Friedel pairs and were classed as strong. 8.7% had negative intensities (less than the background). The remaining 58% of reflections were classed as weak. From the optical density of diffraction spots, we estimated that about 1,000 electrons contributed to one strong reflection. A weak spot thus contains fewer than 100 electrons. The averaged R_{sym} for all the patterns in the 3D data set was 21.8%, very similar to the corresponding value of 21.3% for untitled patterns (Table 1). The R_{sym} and, hence, the overall quality of diffraction patterns was thus nearly independent of the tilt angle. The overall R_m of the whole data set was 27.6%, indicating good consistency between measurements from different films. Again, R_m was similar for patterns recorded at different tilt angles (Table 1). The highest actual tilt angle was 58.7°. The angles of the tilt axis with the reciprocal lattice were randomly distributed in the asymmetric unit, ensuring a complete sampling of 3D Fourier space except for the missing cone.

Due to the two-dimensional nature of the crystals, the structure factors are continuous along lattice lines in the direction normal to the crystal plane (z^*-direction; Henderson and Unwin, 1975). There are 375 (h, k, z^*) lattice lines in the asymmetric unit of LHC-II crystals between 30.0 and 3.2 Å resolution, three of which are shown in Fig. 3. In the $p321$ layer group, lattice lines with indices (h, h, z^*) on the unit cell diagonal are mirror symmetric about the $z^* = 0$ plane. The intensity along these lattice lines was entirely symmetric (Fig. 3 *a*). For

TABLE 1 Three-dimensional data set of electron diffraction intensities from LHC-II

Tilt angles	Number of patterns	Measured Friedel pairs	R_{sym} (%)	R_m (%)
0°	18	30,660	21.3	26.6
20°	7	12,729	18.6	27.1
45°	10	10,290	22.5	27.2
60°	48	39,501	23.0	28.9
Total	83	93,180	21.8	27.6

83 out of 1,200 diffraction patterns recorded from LHC-II crystals tilted up to 60° were processed and merged. R_{sym} is the Friedel symmetry R-factor, and R_m is the merging R-factor (see Materials and Methods). Note that the R-factors do not vary much with tilt angle.

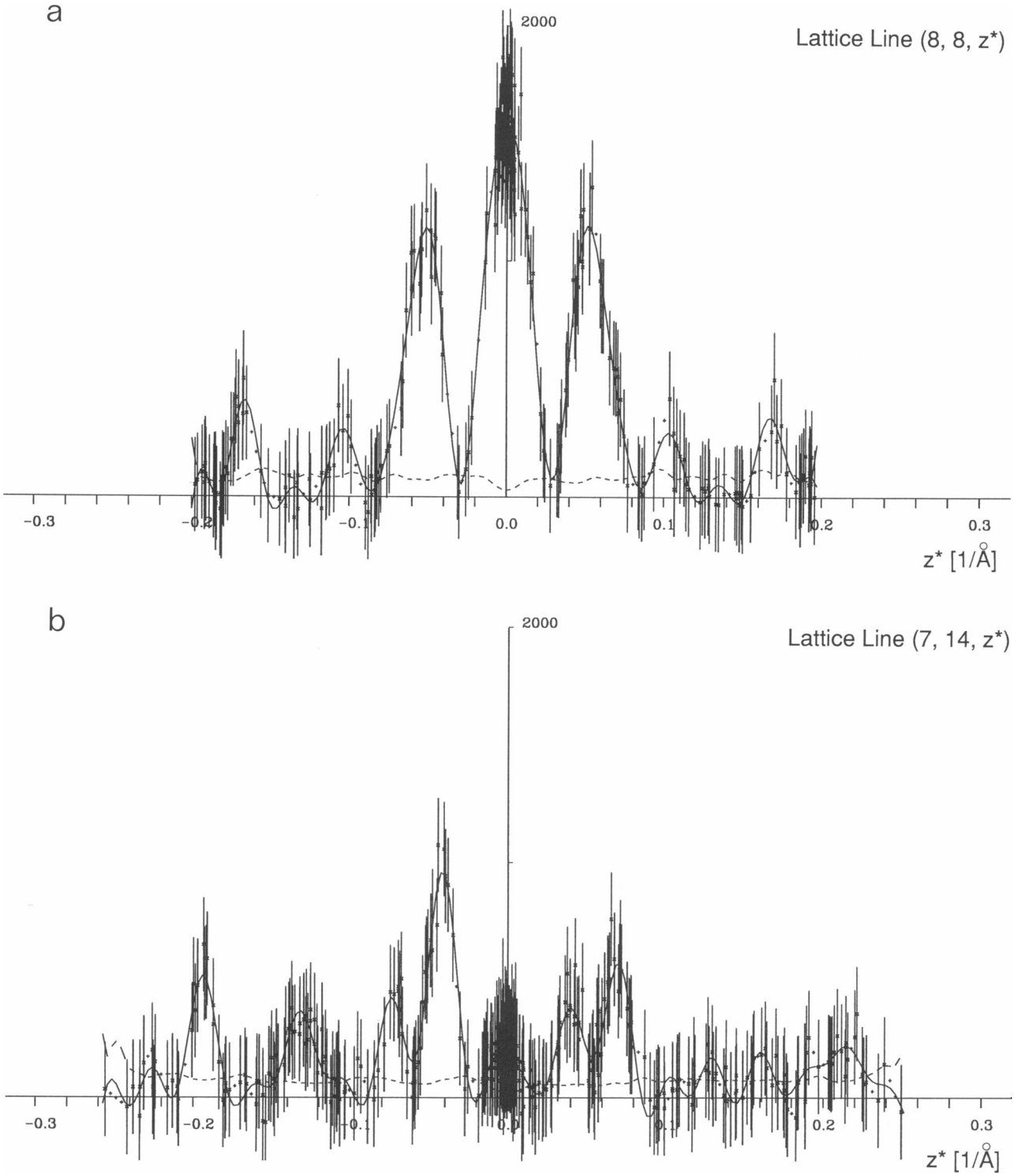
a
2000
Lattice Line (8, 8, z*)
−0.3
−0.2
−0.1
0.0
0.1
0.2
0.3
z* [1/Å]
b
2000
Lattice Line (7, 14, z*)
−0.3
−0.2
−0.1
0.0
0.1
0.2
0.3
z* [1/Å]

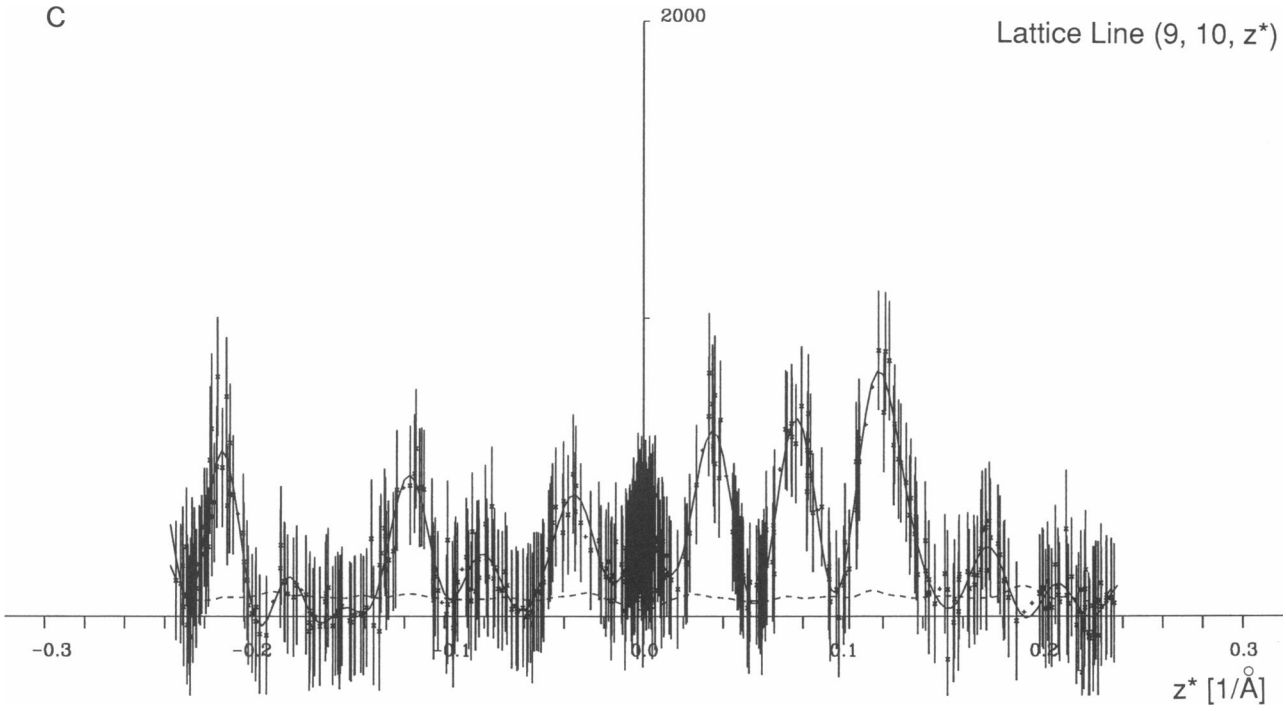

FIGURE 3. Three representative lattice lines (*a*) (8, 8, z^*), (*b*) (7, 14, z^*) and (*c*) (9, 10, z^*) out of 375 in the merged data set. The error bars represent the intensity difference between pairs of reflections related by Friedel symmetry. The solid line is the fitted curve. The dashed line indicates the error between the fitted curve and the measurement which is higher in regions where the reciprocal space is less well sampled. In the $p321$ layer group, lattice lines (h, h, z^*) should be mirror symmetric about the $z^* = 0$ plane. Lattice line (8, 8, z^*) is shown here before imposing this symmetry.

the 17 lattice lines with indices (h, h, z^*), the R-factor between the two halves is 17.4%. This indicates the absence of distortions of the crystal structure that might arise from one-sided interaction with tannin or with the carbon support film.

Each diffraction pattern represents a central section through the 3D reciprocal lattice by the Ewald sphere. According to Klug and Crowther (1972), the number N of evenly-spaced central sections required to determine the structure of a object with a diameter d at resolution r, is $N = \pi \times d/(n \times r)$, where n is a factor equal to the product of all crystallographic and noncrystallographic symmetries, in this case, 6. With perfect, noise-free data, 10 evenly-spaced diffraction patterns should suffice to sample the whole reciprocal space to 3.0 Å resolution for a particle with dimensions of a LHC-II monomer. In practice, many more measurements are required, especially with data of low signal-to-noise ratio. The number of data points in the current 3D set is more than adequate to follow the intensity profile of lattice lines reliably (Fig. 3). Including more diffraction patterns of the same quality will reduce the R-factors, though, and result in more accurate amplitudes of structure factors.

Distribution of intensity in 3D and structure of the complex

Metal-shadowing of freeze-dried 2D LHC-II crystals revealed a thickness of 60 Å (Kühlbrandt, 1984). A sampling distance of 1/140 $Å^{-1}$ in z^* direction, slightly smaller than the maximum distance required by the sampling theorem (Korn and Korn, 1968), was used. This yielded 17,920 structure factor intensities. The 3D distribution of intensities in reciprocal space was investigated by projecting the asymmetric unit in reciprocal space rotationally about the z^*-axis (Fig. 4). Data extended to 3.2 Å resolution in all directions except for a missing cone of 31.3°. This meant that 85.4% of reciprocal space in the resolution range between 30.0 and 3.2 Å was mapped. The projection indicated that most of the diffracted intensity was distributed more or less evenly in two lobes between 30 and 3.7 Å resolution. These lobes were centered around the $z^* = 0$ plane and separated by an arc of lower intensity ranging from 6.6 to 5.5 Å resolution. Vertically, the strong intensity extended to $\sim \pm 1/7.5$ $Å^{-1}$. In this range, there were no extensive regions of low intensity which are characteristic of the

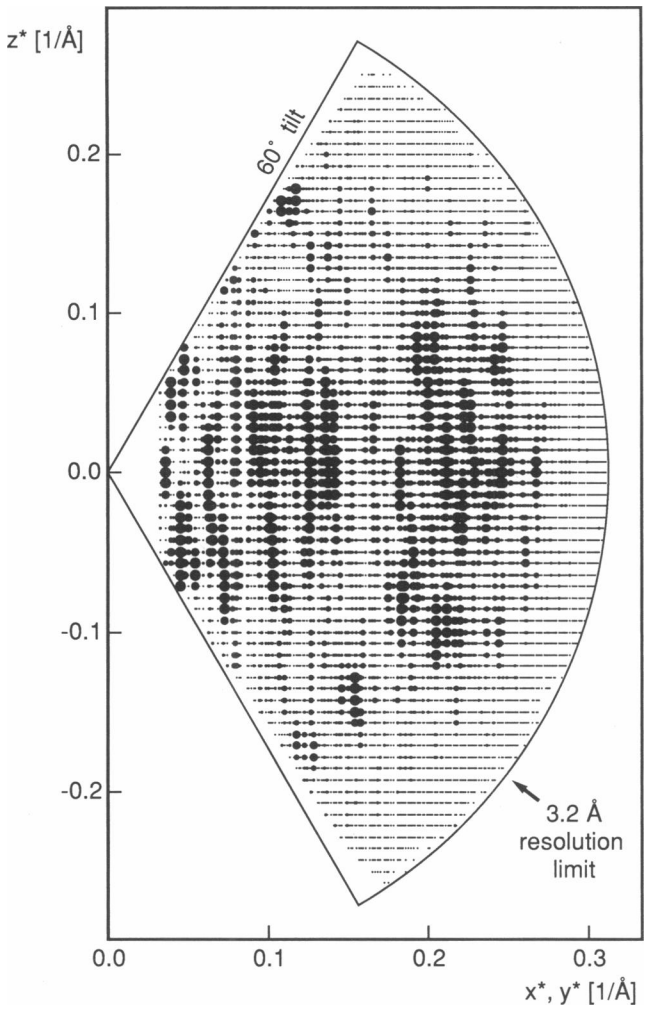

FIGURE 4. Distribution of diffracted intensity in the three-dimensional data set. Lattice lines were sampled at 1/140 $Å^{-1}$ and projected rotationally about the z^*-axis normal to the x^*, y^* -plane which coincides with the membrane plane. The intensity at each sampling point is proportional to the diameter of the dots. The largest dots correspond to intensities $> 8 \times \Delta I_F$, the smallest dots to intensities less than $2 \times \Delta I_F$, where ΔI_F is the average intensity difference between Friedel pairs. There are two large clusters of high intensity in the 30–3.7 Å resolution range centered around the x^*, y^*-plane and several small islands at high z^* in the 5.2–4.7 Å resolution range.

3D electron diffraction of purple membrane (Baldwin and Henderson, 1984; Ceska and Henderson, 1990) and PhoE porin (Walian and Jap, 1990). The clustering of diffraction intensity in the broad arc around 4 Å resolution which is not observed in the 3D diffraction intensities of the other two membrane proteins may arise from the interatomic spacings within chlorophyll molecules.

Fig. 4 is a rotational projection of all 375 lattice lines in the asymmetric unit onto the (x^*, z^*) plane. Only few have a maximum at $z^* = 0$. Therefore, 2D crystals of LHC-II cannot be approximated as a smooth sheet of uniform thickness, even at low resolution. The density within the crystals must be more highly modulated in z-direction than that of purple membrane and PhoE porin. The width of peaks of intensity on most lattice lines of 0.033 ± 0.005 $Å^{-1}$ indicates that the main density of the complex is confined to features of ~30 ± 5 Å thickness. This is, in fact, observed in a 3D map of the complex at 6 Å resolution (Külbrandt and Wang, 1991). The main density of three transmembrane α-helices and of porphyrin head groups is found within the thickness of the hydrophobic part of the membrane which measures 30 Å.

The axial reflections of an oriented pellet of 2D crystals of LHC-II measured by low angle x-ray diffraction indicated a stacking repeat of 76± 3 Å (Kühlbrandt, 1988). This is somewhat larger than the 60 Å thickness of the complex, probably due to the presence of hydration layers. The strong second and third order diffraction maxima of the stacking repeat, at periodicities of 36 and 25 Å, are consistent with a lamellar density distribution within the complex, due to the arrangement of the chlorophyll head groups in two layers (Kühlbrandt and Wang, 1991).

Sources of experimental error

A critical assessment of the errors of measurement and their sources is particularly important if, as in this case, the signal-to-noise ratio of the majority of reflections is low. The overall R_m of 27.6% compares well with those obtained with bacteriorhodopsin (Ceska and Henderson, 1990) and PhoE porin (Walian and Jap, 1990) for which R_m of 15% and 39% have been reported, respectively. The 3D data set of electron diffraction intensities of purple membrane, collected by Ceska and Henderson (1990) contained data from 150 crystals. Because of the lower $p3$ symmetry of purple membrane, this data set is similar to ours in terms of the number of measurements per lattice line. Therefore, the overall R_m of the two data sets can be compared directly. The average intensity of reflections recorded from purple membrane is ~7× stronger than that of 2D crystals of LHC-II of similar size (Wang and Kühlbrandt, 1991). According to Eq. 4, the ratio between the overall R_m of the two data sets should be ~2.64. The higher R_m of our data set is thus fully accounted for by the weaker average intensity of reflections from LHC-II crystals. In fact, the ratio between the R_m in the two cases is 1.84, and thus much better than expected, probably due to the occurrence of twinning in the purple membrane and the use of thicker carbon support films, causing higher background intensities (Ceska and Henderson, 1990).

The R_m for electron diffraction data obtained so far is

significantly higher than the equivalent in x-ray crystallography, referred to as measurement reliability (Blundell and Johnson, 1976), which is typically ~5% for a 3D protein crystal. Apart from the sources of experimental error identified by Ceska and Henderson (1990), namely, (*a*) the curvature of the Ewald sphere, (*b*) dynamical scattering of electrons and (*c*) the blurring of spots perpendicular to the tilt axis, there are two other major factors to account for the large difference in the accuracy of electron and x-ray diffraction data, related to the number of unit cells and to the electron dose.

A 2D crystal of LHC-II measuring 8 μm across contains 3.6×10^5 unit cells. Our 3D set of intensity data contains information collected from a total of $\sim 3 \times 10^7$ unit cells. By comparison, a typical protein crystal used in x-ray crystallography has a size of 0.2 to 0.5 mm in three dimensions, containing at least 10^{13} to 10^{14} unit cells. The difference in crystal size and, consequently, of the number of unit cells contributing to the diffraction pattern, is a principal factor responsible for the observed discrepancies in the relative accuracy of measurements. The number of unit cells is a serious limitation, even though atomic scattering factors for electrons are ~10,000 × higher than for x-rays (Appendix) and the 2D crystals used for electron diffraction have little or no mosaicity. Tivol et al. (1982) have shown that 3D crystals of hemoglobin with a thickness of 1,600 Å yield highly accurate electron diffraction intensities, with R_{sym} of 5% and R_m of 5.6%. However, with such thin 3D crystals, dynamical scattering has to be taken into consideration which means that structure factors cannot be derived easily from the electron diffraction intensities (Jap and Glaeser, 1978; Glaeser and Ceska, 1989).

A 3D protein crystal can normally be kept in the x-ray beam for hours or days so that a complete 3D data set is collected from a single crystal, without significant loss of high-resolution structural information. This means the radiation dose is high enough for the statistical error to become less significant than the systematical error. For an electron diffraction pattern, Eq. 4 indicates that a 5% *R*-factor would require every reflection to contain, on average, 400 electrons. The cross-section for inelastic electron scattering is at least twice as high as for elastic scattering for unstained biological materials at any scattering angle (Reimer, 1989). Electrons scattered inelastically by the crystal spread over the whole Fourier space, as are electrons scattered elastically and inelastically from the solvent in the crystal and from the carbon support film (Fig. 2). These intensity contributions to the diffraction peaks can be subtracted by background correction, but the statistical error introduced by these sources remains. Taking this into consideration, the average number of electrons required for a 5% *R*-factor would probably be several times higher than 400. The majority of reflections from LHC-II 2D crystals contain only ~100 electrons, resulting in larger *R*-factors.

In x-ray crystallography, the measurement reliability, an *R*-factor based on intensity, is always used when referring the accuracy of diffraction intensities. However, when referring to the agreement between a structural model and the experimental data, an *R*-factor based on amplitude (i.e., the crystallographic *R*-factor) is used. An intensity-based *R*-factor would be higher by a factor of two. The ratio between electron and x-ray intensities is related to the square of the corresponding atomic scattering factors. However, as shown in Eq. 5, the *R*-factor is inversely proportional to the scattering factor but not to its square. Therefore, in this case the measurement accuracy is compared in terms of atomic scattering amplitudes.

For the highest signal-to-noise ratio of electron diffraction peaks, the desired electron dose is that which a crystal can withstand before high resolution information is lost due to radiation damage. Unwin and Henderson (1975) have defined a critical dose N_e as the dose that reduces the fastest-fading spots to 1/e of their initial intensities. It was found that for high resolution spots N_e is lower (Hayward and Glaeser, 1979), presumably because chemical bonds break before any mass loss occurs. A factor of 4–5 is gained in by cooling protein crystals from the room temperature to −120°C (Hayward and Glaeser, 1979; International Experimental Study Group, 1986). From the optical density of micrograph recorded at identical conditions, the critical dose for reflections of LHC-II crystals at 4 Å resolution or higher was found to be ~3–5 electrons/Å^2 at −125°C. This value is similar to the dose found for purple membrane at −120°C (T. Ceska, personal communication). All high-resolution diffraction patterns in this study were recorded at this dose. Intensities of low-order reflections were measured at a lower dose.

Because the statistical error of measurements is inversely proportional to the diameter of the diffracting area (see Eq. 5), we estimate that 2D crystals of LHC-II of 40–50 μm diameter are required for collecting reflection intensities with an accuracy comparable to x-ray crystallography. However, the experimental difficulty of preparing such large 2D crystals for electron microscopy with the necessary high degree of flatness would be extreme, even if the crystals can be grown to this size. Alternatively, a much larger number (perhaps as many as 2,000) diffraction patterns of the smaller 2D crystals currently available will be needed. With a data set of this quality, phasing methods which are routinely used with x-rays should all become possible in electron crystallography.

APPENDIX

Comparison of X-Ray and Electron Atomic Scattering Factors

L.C. Qin
Massachusetts Institute of Technology, Cambridge, Massachusetts 02139, USA

When an incident plane wave of unit amplitude propagating along the z direction described by wave function $\psi_0 = \exp(2\pi ikz)$ is elastically scattered by an atom, the far field solution ψ is often expressed in the form of

$$\psi = \psi_0 + \frac{\phi}{r}\exp(2\pi kr),$$

where $k = 1/\lambda$ is the wave number (magnitude of wave vector $\vec{k}$ with λ being the wavelength), and ϕ is the amplitude of the scattered spherical wave. It can be seen from the above equation that the unit of ϕ is the unit of length, the same as that of r.

In the case of fast electron scattering,

$$\phi = f^{(B)},$$

where $f^{(B)}$ is also called the atomic scattering amplitude for electrons (International Tables for X-Ray Crystallography, 1974). Under the Born approximation,

$$f^{(B)} = \frac{2\pi me}{h^2}\int v(\vec{r})\exp(-2\pi i\vec{k}\cdot r)\,d\vec{r},$$

where $v(\vec{r})$ is the atomic coulombic potential function, h is Planck's constant, and m and e are the relativistic mass of the electron and the absolute value of the electrical charge of the electron, respectively.

But in the case of x-ray scattering, due to historical reasons (Thomson formula) (James, 1962), the scattering amplitude (neglecting polarization effects and Compton scattering) is expressed in the following form:

$$\phi = -\frac{e^2}{mc^2}f^{(X)} = -r_e f^{(X)}$$

where c is the speed of light, $r_e = e^2/mc^2 = 2.818 \times 10^{-13}$ cm is the classical electron radius, and $f^{(X)}$ is conventionally referred to as the atomic scattering amplitude for x-rays (International Tables for X-Ray Crystallography, 1974),

$$f^{(X)} = \int \rho_e(\vec{r})\exp(-2\pi i\vec{k}\cdot\vec{r})^{d\vec{r}}$$

where $\rho_e(\vec{r})$ is the electron density function of the atom.

Therefore, when $f^{(B)}$ and $f^{(X)}$ are compared to each other, $r_e f^{(X)}$ should be used.

From this it can be seen that the atomic scattering amplitudes of light elements for fast electrons have values of $0.5 \sim 2.5$ Å and of $\sim 10^{-4}$ Å for x-rays (International Tables for X-Ray Crystallography, 1974).

APPENDIX REFERENCES

International Tables for X-Ray Crystallography. Vol. IV. 1974. The Kynoch Press, Birmingham, England. 71–175.

James, R. W. 1962. The Optical Principles of the Diffraction of X-Rays. Bell and Sons, London. 29–31.

We thank Karoline Dörr for isolating the complex, Tom Ceska for discussions on processing, Kevin Leonard for advice on computing, Richard Henderson for programs for processing electron diffraction patterns, and Bob Glaeser for advice on specimen preparation.

Financial support from the Deutsche Forschungsgemeinschaft (DFG) is gratefully acknowledged.

Received for publication 22 April 1991 and in final form 4 September 1991.

REFERENCES

Baldwin, J. M., and R. Henderson. 1984. Measurement and evaluation of electron diffraction patterns from two-dimensional crystals. *Ultramicroscopy.* 14:319–335.

Blundell, T. L., and L. N. Johnson. 1976. Protein Crystallography. Academic Press, London. 240–336.

Butler, P. J. G., and W. Kühlbrandt. 1988. Determination of the aggregate size in detergent solution of the light-harvesting chlorophyll *a*/*b*-protein complex from chloroplast membranes. *Proc. Natl. Acad. Sci. USA.* 85:3797–3801.

Butt, H.-J., D. N. Wang, P. K. Hansma, and W. Kühlbrandt. 1991. Effect of surface roughness of carbon support films on high-resolution electron diffraction of two-dimensional protein crystals. *Ultramicroscopy.* 36:307–318.

Ceska, T. A., and R. Henderson. 1990. Analysis of high-resolution electron diffraction patterns form purple membrane labelled with heavy-atoms. *J. Mol. Biol.* 213:539–560.

Dubochet, J., M. Adrian, J.-J. Chang, J.-C. Homo, J. Lepault, A. W. McDowall, and P. Schultz. 1988. Cryo-electron microscopy of vitrified specimens. *Quart. Rev. Biophys.* 21:129–228.

Glaeser, R. M., and T. A. Ceska. 1989. High-voltage electron diffraction from bacteriorhodopsin (purple membrane) is measurably dynamical. *Acta Cryst.* A45:620–628.

Hayward, B., and R. M. Glaeser. 1979. Radiation damage of purple membrane at low temperature. *Ultramicroscopy.* 4:201–210.

Henderson, R., and P. N. T. Unwin. 1975. Three-dimensional model of purple membrane obtained by electron microscopy. *Nature (Lond.).* 257:28–32.

Ho, M.-H., B. K. Jap, and R. M. Glaeser. 1988. Validity domain of the weak-phase-object approximation for electron diffraction of thin protein crystals. *Acta Cryst.* A44:878–884.

International Experimental Study Group. 1986. Cryoprotection in electron microscopy. *J. Microsc.* 141:385–391.

International Tables for X-ray Crystallography. Vol. IV. 1974. The Kynoch Press, Birmingham, England. 71–175.

Jap, B. K., and R. M. Glaeser. 1978. The scattering of high-energy electrons. I. Feynman path-integral formation. *Acta Cryst.* A34:94–102.

Klug, A., and R. A. Crowther. 1972. Three-dimensional image reconstruction from the viewpoint of information theory. *Nature (Lond.).* 238:435–440.

Korn, G. A., and T. M. Korn. 1968. Mathematical Handbook for Scientists and Engineers. McGraw-Hill, New York. 630–654.

Kühlbrandt, W. 1984. Three-dimensional structure of the light-harvesting chlorophyll *a*/*b* protein complex from pea chloroplasts. *Nature (Lond.)*. 307:478–480.

Kühlbrandt, W. 1987. Photosynthetic membrane and membrane proteins. *In* Electron Microscopy of Proteins, Vol. 6. J. R. Harris, and R. W. Horne, editors, Academic Press, London. 155–207.

Kühlbrandt, W. 1988. Structure of light-harvesting chlorophyll *a*/*b* protein complex from plant photosynthetic membranes at 7 Å resolution in projection. *J. Mol. Biol.* 202:849–864.

Kühlbrandt, W., and K. Downing. 1989. Two-dimensional structure of plant light-harvesting complex at 3.7 Å resolution by electron crystallography. *J. Mol. Biol.* 207:823–828.

Kühlbrandt, W., T. Thaler, and E. Wehrli. 1983. The structure of membrane crystals of the light-harvesting chlorophyll *a*/*b*-protein complex. *J. Cell. Biol.* 96:1414–1424.

Kühlbrandt, W., and D. N. Wang. 1991. Three-dimensional structure of plant light-harvesting complex determined by electron crystallography. *Nature (Lond.)*. 350:130–134.

Reimer, L. 1989. Transmission Electron Microscopy. 2nd edition, Springer-Verlag, Heidelberg. 136–191.

Shaw, P. J., and G. J. Hills. 1981. Tilted specimen in the electron microscope: a simple specimen holder and the calculation of tilt angles for crystalline specimens. *Micron.* 12:279–282.

Staehelin, L. A. 1986. Chloroplast structure and supermolecular organization of photosynthetic membranes. *In* Encyclopaedia of Plant Physiology. Vol. 19. L. A. Staehelin, and C. J. Arntzen, editors. Springer, Heidelberg. 1–84.

Thornber, J. P. 1986. Biochemical characterization and structure of pigment-proteins of photosynthetic organisms. *In* Encyclopaedia Plant Physiology. Vol. 19. L. A. Staehelin, and C. J. Arntzen, editors. Springer, Heidelberg. 98–142.

Tivol, W. F., B.-W. B. Chang, and D. F. Parsons. 1982. Reproducibility of electron diffraction intensity data obtained from hydrated microcrystals of rat hemoglobin. *Ultramicroscopy.* 9:117–130.

Walian, P., and B. K. Jap. 1990. Three-dimensional electron diffraction of PhoE Porin to 2.8 Å resolution. *J. Mol. Biol.* 215:429–438.

Wang, D. N., and W. Kühlbrandt. 1991. High-resolution electron crystallography of light-harvesting chlorophyll *a*/*b*-protein complex in three different media. *J. Mol. Biol.* 217:691–699.

Unwin, P. N. T., and R. Henderson. 1975. Molecular structure determination by electron microscopy of unstained specimens. *J. Mol. Biol.* 94:425–440.